

## Spin-Spiral States in Undoped Manganites: Role of Finite Hund's Rule Coupling

Sanjeev Kumar,<sup>1,2</sup> Jeroen van den Brink,<sup>1,3,4,5</sup> and Arno P. Kampf<sup>6</sup>

<sup>1</sup>*Institute Lorentz for Theoretical Physics, Leiden University, P.O. Box 9506, 2300 RA Leiden, The Netherlands*

<sup>2</sup>*Faculty of Science and Technology, University of Twente, P.O. Box 217, 7500 AE Enschede, The Netherlands*

<sup>3</sup>*Institute for Molecules and Materials, Radboud Universiteit Nijmegen, P.O. Box 9010, 6500 GL Nijmegen, The Netherlands*

<sup>4</sup>*Stanford Institute for Materials and Energy Sciences, Stanford University and SLAC National Accelerator Laboratory, Menlo Park, California 94025, USA*

<sup>5</sup>*Leibniz-Institute for Solid State and Materials Research Dresden, D-01171 Dresden, Germany*

<sup>6</sup>*Theoretical Physics III, Electronic Correlations and Magnetism, University of Augsburg, D-86135 Augsburg, Germany*

(Received 29 May 2009; published 4 January 2010)

The experimental observation of multiferroic behavior in perovskite manganites with a spiral spin structure requires a clarification of the origin of these magnetic states and their relation to ferroelectricity. We show that spin-spiral phases with a diagonal wave vector and also an  $E$ -type phase exist for intermediate value of Hund's rule and the Jahn-Teller coupling in the orbitally ordered and insulating state of the standard two-band model Hamiltonian for manganites. Our results support the spin-current mechanism for ferroelectricity and present an alternative view to earlier conclusions where frustrating superexchange couplings were crucial to obtaining spin-spiral states.

DOI: 10.1103/PhysRevLett.104.017201

PACS numbers: 75.47.Lx, 75.10.-b, 75.80.+q, 77.80.-e

The coexistence of long-range magnetic order with spontaneous electric polarization is commonly referred to as multiferroic behavior [1]. In recent years multiferroic materials have attracted special attention from the condensed matter community because of their potential for applications in memory and data storage devices [2,3]. Despite the initial observation that materials with coexisting ferroelectric and magnetic orders are rare in nature [4], an increasing number of multiferroic materials with interesting properties has been discovered [5–8]. Different mechanisms for the origin of multiferroic behavior have been proposed and partially identified [9–14]. In a selected class of multiferroics ferroelectricity is driven by the existence of a nontrivial magnetic order, e.g., with a spiral spin structure [15–18]. It has therefore become a key issue to clarify the conditions under which nontrivial spin states can occur in different models and materials.

Hole-doped perovskite manganites are known for their rich phase diagrams and complex transport phenomena [19]. The recent observations of ferroelectricity in  $\text{TbMnO}_3$  and  $\text{DyMnO}_3$  stimulated further research also on the undoped materials. The magnetic ground state of  $\text{RMnO}_3$  with  $R = \text{La, Pr, Nd, and Sm}$  is an  $A$ -type antiferromagnet (AFM), with ferromagnetic (FM) order in the  $a$ - $b$  plane and a staggered spin pattern along the  $c$  axis. It changes to a spiral magnet for  $R = \text{Tb and Dy}$ , and finally to an  $E$ -type AFM for  $R = \text{Ho}$ , where zigzag FM chains alternate in their preferred spin direction [17,20]. Although the  $A$ -type order of the prototype compound  $\text{LaMnO}_3$  is well understood in terms of Goodenough-Kanamori rules and orbital ordering [19], the magnetic structure of the materials with smaller ionic radii are much less understood. It was proposed that due to  $\text{GdFeO}_3$ -type structural

distortions longer-range interactions become relevant and thereby may lead to complex magnetic ground states with spiral or  $E$ -type spin patterns [17,21]. The existence of an  $E$ -type pattern in these models with longer-range interactions has been put into question recently [22].

In this Letter we explore the magnetic ground states in a two-band model for  $\text{RMnO}_3$  without invoking the next-nearest neighbor or even longer-range interactions. The model consists of itinerant electrons coupled locally to core spins via Hund's rule coupling  $J_H$ , and a nearest-neighbor antiferromagnetic interaction between the spins. Importantly, we refrain from taking the commonly adopted double-exchange limit  $J_H \rightarrow \infty$ . The two-orbital nature of the model allows for the inclusion of the Jahn-Teller (JT) distortions as a source for orbital order and hence the insulating character of the undoped manganites. We find that both the spiral spin states and the  $E$ -type states are stable in the parameter regime relevant for manganites. The experimentally observed transitions between different magnetic states are obtained only for finite JT couplings and intermediate values of  $J_H$ .

Specifically, we consider a two-dimensional two-band model with the Hamiltonian [23]:

$$H = - \sum_{\langle ij \rangle \sigma}^{\alpha \beta} t_{\alpha \beta} (c_{i\alpha\sigma}^\dagger c_{j\beta\sigma} + \text{H.c.}) - J_H \sum_{i\alpha} \mathbf{S}_i \cdot \boldsymbol{\sigma}_{i\alpha} + J_s \sum_{\langle ij \rangle} \mathbf{S}_i \cdot \mathbf{S}_j \quad (1)$$

at quarter filling to describe the undoped manganites  $\text{RMnO}_3$ . Here,  $c_{i\alpha\sigma}$  and  $c_{i\alpha\sigma}^\dagger$  are annihilation and creation operators for electrons with spin  $\sigma$  in the  $e_g$  orbital  $\alpha \in \{x^2 - y^2, 3z^2 - r^2\}$ , which from here onwards is labeled as

1 and 2, respectively.  $t_{\alpha\beta}^{ij}$  denote the hopping amplitudes between the two  $e_g$  orbitals on nearest-neighbor sites and have the cubic perovskite specific form [19]:  $t_{11}^x = t_{11}^y \equiv t$ ,  $t_{22}^x = t_{22}^y \equiv t/3$ ,  $t_{12}^x = t_{21}^x \equiv -t/\sqrt{3}$ ,  $t_{12}^y = t_{21}^y \equiv t/\sqrt{3}$ , where  $x$  and  $y$  mark the spatial directions. In a commonly used approximation for manganites, the core spins are treated as classical vectors with  $|\mathbf{S}| = 1$ ; the justification of this approximation was quantitatively verified [24].  $\sigma_{i\alpha}$  denotes the electronic spin operator defined as  $\sigma_{i\alpha}^\mu = \sum_{\sigma\sigma'} c_{i\alpha\sigma}^\dagger \Gamma_{\sigma\sigma'}^\mu c_{i\alpha\sigma'}$ , where  $\Gamma^\mu$  are the Pauli matrices. The one-band version of the above model and the Kondo lattice model with  $J_s = 0$  have been previously analyzed in one and two dimensions in search for nontrivial magnetic ground states [25–28]. Although spin-spiral states were found for selected combinations of band fillings and Hund's rule coupling, the connection to the spin spirals observed in the  $RMnO_3$  is unclear since the insulating character of orbitally ordered  $RMnO_3$  is not captured by the one-band models.

By applying a canonical transformation we rewrite the Hamiltonian in a basis where the spin-quantization axis is site-dependent and points along the direction of the local core spin. Introducing polar and azimuthal angles  $\theta$  and  $\phi$ , respectively, the transformation is defined as

$$\begin{aligned} \begin{bmatrix} c_{i\alpha\uparrow} \\ c_{i\alpha\downarrow} \end{bmatrix} &= \begin{bmatrix} \cos(\frac{\theta_i}{2})e^{i\phi_i/2} & -\sin(\frac{\theta_i}{2})e^{i\phi_i/2} \\ \sin(\frac{\theta_i}{2})e^{-i\phi_i/2} & \cos(\frac{\theta_i}{2})e^{-i\phi_i/2} \end{bmatrix} \begin{bmatrix} d_{i\alpha p} \\ d_{i\alpha a} \end{bmatrix} \\ &\equiv \mathcal{U}(\theta_i, \phi_i) \begin{bmatrix} d_{i\alpha p} \\ d_{i\alpha a} \end{bmatrix}. \end{aligned} \quad (2)$$

Here  $d_{i\alpha p}$  ( $d_{i\alpha a}$ ) annihilates an electron at site  $i$  in orbital  $\alpha$  with spin parallel (antiparallel) to the core spin. In terms of  $d$  operators the Hamiltonian reads:

$$\begin{aligned} H &= - \sum_{\langle ij \rangle} \sum_{\sigma, \sigma'} t_{\alpha\beta} f_{\sigma\sigma'} d_{i\alpha\sigma}^\dagger d_{j\beta\sigma'} + \text{H.c.} \\ &\quad - \frac{J_H}{2} \sum_{i\alpha} (n_{i\alpha p} - n_{i\alpha a}) + J_s \sum_{\langle ij \rangle} \mathbf{S}_i \cdot \mathbf{S}_j, \end{aligned} \quad (3)$$

with  $n_{i\alpha s} = d_{i\alpha s}^\dagger d_{i\alpha s}$ . The coefficients  $f_{\sigma\sigma'}$  are explicitly given by,

$$\begin{bmatrix} f_{pp} & f_{pa} \\ f_{ap} & f_{aa} \end{bmatrix} = \mathcal{U}^\dagger(\theta_i, \phi_i) \cdot \mathcal{U}(\theta_j, \phi_j). \quad (4)$$

The advantage of this transformation is that the Hund's rule term now becomes diagonal. For a fixed configuration of classical spins the Hamiltonian is bilinear in the fermion operators. However, the one-particle Schrödinger equation cannot be solved in closed form for an arbitrary spin configuration. We therefore selectively analyze the core spin configurations described by the polar and azimuthal angles  $\theta_i = \Theta$  and  $\phi_i = \mathbf{q} \cdot \mathbf{r}_i$ . We refer to  $\Theta$  as the cone angle and  $\mathbf{q}$  as the spiral wave vector. Despite this restriction most of the well-known spin patterns as observed in various magnetic materials are included, e.g., ferromag-

netic, antiferromagnetic, canted-ferromagnetic, and spin-spiral patterns.

For this choice of variational spin states the Hamiltonian matrix reduces to a  $4 \times 4$  matrix after Fourier transformation with  $d_{i\alpha s} = N^{-1/2} \sum_{\mathbf{k}} e^{-i\mathbf{k} \cdot \mathbf{r}_i} d_{\mathbf{k}\alpha s}$ , and the kinetic energy term in Eq. (3) is then written as  $H_{\text{kin}} = \sum_{\mathbf{k}} \mathbf{D}_{\mathbf{k}}^\dagger \mathcal{H}(\mathbf{k}) \mathbf{D}_{\mathbf{k}}$ , where  $\mathbf{D}_{\mathbf{k}}^\dagger \equiv [d_{\mathbf{k}1p}^\dagger, d_{\mathbf{k}1a}^\dagger, d_{\mathbf{k}2p}^\dagger, d_{\mathbf{k}2a}^\dagger]$ , and the  $4 \times 4$  matrix  $\mathcal{H}$  is given by

$$\mathcal{H}(\mathbf{k}) \equiv \begin{bmatrix} h_{11}^{pp} & h_{11}^{pa} & h_{12}^{pp} & h_{12}^{pa} \\ h_{11}^{ap} & h_{11}^{aa} & h_{12}^{ap} & h_{12}^{aa} \\ h_{21}^{pp} & h_{21}^{pa} & h_{22}^{pp} & h_{22}^{pa} \\ h_{21}^{ap} & h_{21}^{aa} & h_{22}^{ap} & h_{22}^{aa} \end{bmatrix}, \quad (5)$$

with the matrix elements,

$$\begin{aligned} h_{\alpha\beta}^{pp} &= \sum_{\mu=x,y} t_{\alpha\beta}^\mu \left[ \cos^2\left(\frac{\Theta}{2}\right) \cos k_\mu^+ + \sin^2\left(\frac{\Theta}{2}\right) \cos k_\mu^- \right] \\ h_{\alpha\beta}^{aa} &= \sum_{\mu=x,y} t_{\alpha\beta}^\mu \left[ \cos^2\left(\frac{\Theta}{2}\right) \cos k_\mu^+ + \sin^2\left(\frac{\Theta}{2}\right) \cos k_\mu^- \right] \\ h_{\alpha\beta}^{ap} &= \sum_{\mu=x,y} t_{\alpha\beta}^\mu \sin(\Theta) \sin\left(\frac{q_\mu}{2}\right) \sin k_\mu = h_{\alpha\beta}^{pa}, \end{aligned} \quad (6)$$

with  $k_\mu^\pm = k_\mu \pm q_\mu/2$ . For a single band  $H_{\text{kin}}$  reduces to a  $2 \times 2$  matrix structure and therefore the eigenspectrum is straightforwardly obtained in a closed form expression [25]. For the two-band case considered here the closed form result for the dispersion is rather involved and we therefore diagonalize the above  $4 \times 4$  matrix numerically for each momentum  $\mathbf{k}$  on finite lattices of up to  $256 \times 256$  sites.

In Fig. 1 we plot the values of the cone angle  $\Theta$  and spiral wave vector  $(q_x, q_y)$  corresponding to the minimum-energy state as a function of  $J_H$ . Over almost entire parameter regime the cone angle is found to be  $\pi/2$ , which corresponds to planer spin states. Another feature is that  $q_x = q_y$ , suggesting that the diagonal spirals are more stable, which is consistent with the experimental findings [20]. For the diagonal spirals with  $(q_x, q_y) = q(1, 1)$  the spiral pitch  $q$  smoothly vanishes upon reaching the FM state with  $q = 0$ . Close to the FM phase the cone angle of

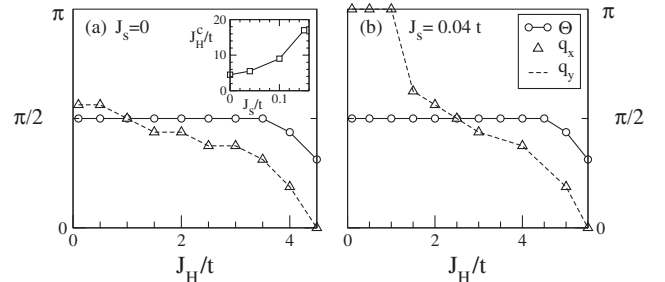


FIG. 1. The cone angle  $\Theta$  and the wave vector  $(q_x, q_y)$  of the lowest-energy spiral state as a function of  $J_H$  for (a)  $J_s = 0$  and (b)  $J_s = 0.04t$ . The inset in (a) shows the  $J_s$  dependence of the critical value of  $J_H$  required to obtain the FM state.

the spiral state slightly deviates from  $\pi/2$ . The ground state jumps discontinuously from an antiferromagnet with  $q = \pi$  to a spiral with  $q < \pi$ . The inset in Fig. 1(a) shows the variation with  $J_s$  of the critical value of Hund's rule coupling  $J_H^c$  for the transition to a ferromagnet.

Before arriving at the magnetic phase diagram of the Hamiltonian, it is essential to consider other states which are not captured by the ansatz  $(\theta_i, \phi_i) = (\Theta, \mathbf{q} \cdot \mathbf{r}_i)$  [26,29]. The energies of the earlier suggested candidate states, including the  $E$ -type states, for the magnetic order in manganites are obtained by exact numerical diagonalization and compared with those of the spiral states.

The ground state phase diagram for the quarter filled system is shown in Fig. 2(a). The  $E$ -type phase is stable in a wide region of parameter space. Spiral states are favored for larger values of  $J_s$ , and also in a narrow window between the FM and the  $E$ -type states. Here, the FM state in a two-dimensional model is representative of a single plane of the  $A$ -type AFM state. In the experiments on  $\text{RMnO}_3$  two transitions are observed, first from the  $A$ -type AFM to the spiral state and subsequently to the  $E$ -type phase, upon reducing the ionic radius of the rare-earth element [17]. Therefore the existence of a direct FM to  $E$ -type transition appears to contradict the experimental observation. Moreover, the phase diagram of Fig. 2(a) corresponds to a metallic state with a finite density of states at the Fermi level; the undoped manganites, however, are insulating. Therefore it is essential to include the source for the opening of an energy gap in the spectrum in order to obtain results applicable to  $\text{RMnO}_3$ . For this purpose we add an adiabatic Jahn-Teller coupling to the Hamiltonian, which is given by

$$H_{\text{JT}} = \lambda \sum_i [Q_{xi} \tau_{xi} + Q_{zi} \tau_{zi}] + \frac{K}{2} \sum_i |\mathbf{Q}_i|^2. \quad (7)$$

In Eq. (7),  $Q_{xi}$  and  $Q_{zi}$  are lattice distortions corresponding to two different JT modes.  $\tau_{xi} = \sum_{\sigma} (c_{i1\sigma}^{\dagger} c_{i2\sigma} + c_{i2\sigma}^{\dagger} c_{i1\sigma})$  and  $\tau_{zi} = \sum_{\sigma} (c_{i1\sigma}^{\dagger} c_{i1\sigma} - c_{i2\sigma}^{\dagger} c_{i2\sigma})$  are orbital pseudospin

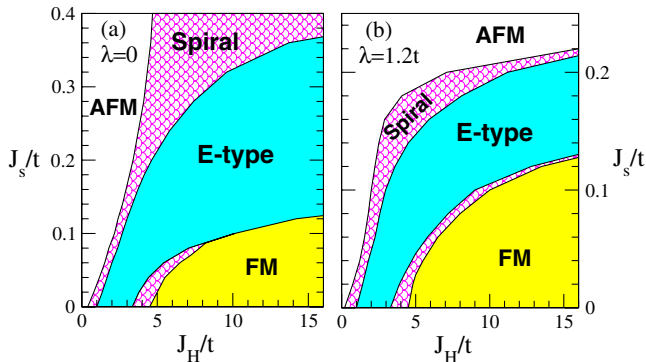


FIG. 2 (color online). Ground state phase diagrams  $J_s$  vs  $J_H$  in the absence (a) and presence (b) of Jahn-Teller distortions. The spiral states have the cone angle  $\Theta = \pi/2$  except in the narrow region between FM and the  $E$ -type states in (a). In both cases  $q_x = q_y$  reduces monotonically as the FM state is approached.

operators [19]. In the undoped manganites staggered JT distortions are accompanied by orbital ordering with transition temperatures much higher than the temperature scale for magnetic ordering [17]. Therefore the pattern for the JT distortions is expected to be robust upon cooling even though the magnitude of the distortions may depend on the magnetic structure. A real-space Monte Carlo study verified the staggered ordering of the  $Q_x$  component when  $H_{\text{JT}}$  is included in the Hamiltonian [30]. Therefore we adopt this pattern for the lattice distortions and set  $Q_{xi} = Q_x^0 e^{i(\pi, \pi) \cdot \mathbf{r}_i}$  and  $Q_{zi} = 0$ . The second term in Eq. (7) is the energy cost associated with the distortion of the lattice with  $|\mathbf{Q}_i|^2 = Q_{xi}^2 + Q_{zi}^2$ . We set the stiffness constant  $K = t$  as in previous theoretical model analyses of manganites [19,30]. We treat  $Q_x^0$  as a variational parameter in the calculations and optimize it by minimizing the total energy. Therefore  $Q_x^0$  is allowed to vary in the different magnetic states.

Because of the staggered orbital order the determination of the eigenspectrum becomes slightly more involved. Instead of a  $4 \times 4$  matrix, we now have to diagonalize the  $8 \times 8$  matrix

$$\begin{bmatrix} \mathcal{H}(\mathbf{k}) & \mathcal{M} \\ \mathcal{M} & \mathcal{H}(\mathbf{k}') \end{bmatrix}$$

for each  $\mathbf{k}$  with  $\mathbf{k}' = \mathbf{k} + (\pi, \pi)$  and

$$\mathcal{M} = \begin{bmatrix} 0 & 0 & 0 & \lambda Q_x^0 \\ 0 & 0 & \lambda Q_x^0 & 0 \\ 0 & \lambda Q_x^0 & 0 & 0 \\ \lambda Q_x^0 & 0 & 0 & 0 \end{bmatrix}. \quad (8)$$

The energy minimization procedure with respect to  $\Theta$  and  $\mathbf{q}$  is followed as before but in the presence of staggered Jahn-Teller distortions, which lead to an insulating state with staggered orbital order. The resulting phase diagram is shown in Fig. 2(b). Remarkably the inclusion of the Jahn-Teller distortions leads to the appearance of spiral states in

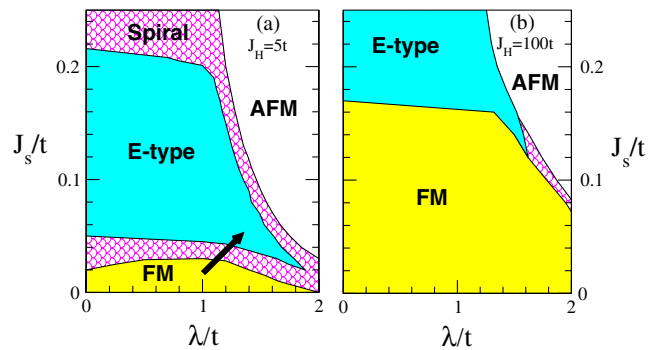


FIG. 3 (color online).  $J_s$ - $\lambda$  phase diagrams for (a)  $J_H = 5t$  and (b)  $J_H = 100t$ . The arrow in (a) is indicative of the path traced upon reducing the ionic radius of the rare-earth ion in  $\text{RMnO}_3$ , which leads to the correct sequence of transitions from FM to spiral to  $E$ -type states. Such a sequence is absent in (b).

between the  $E$ -type and the FM phases in a wide range of the Hund's rule coupling.

An important effect of the size reduction of the rare-earth ion in  $RMnO_3$  is the decrease of the electronic bandwidth due to the Mn-O-Mn bond angle moving further away from  $180^\circ$ . For the model calculations, it is simpler to vary  $J_s$  and  $\lambda$  rather than changing the hopping parameters which control the bandwidth. In Fig. 3 we therefore show the phase diagrams in the parameter space of  $J_s$  and  $\lambda$  for two representative values of  $J_H$ . For  $J_H = 5t$ , the small  $J_s$  regime is ferromagnetic, which describes a single plane of the  $A$ -type AFM observed in  $RMnO_3$  with  $R = \text{La, Pr, Nd, and Sm}$ . A two-step transition occurs from FM via the spiral to the  $E$ -type state by increasing both  $\lambda$  and  $J_s$  [indicated by the arrow in Fig. 3(a)], which effectively translates to reducing the bandwidth. In the (1, 1) spiral state the pitch  $q$  increases along the direction of the arrow [see Fig. 3(a)]. The values of  $q$  at the two end points of the planar spiral phase along the arrow are  $0.13\pi$  and  $0.25\pi$ . These values are close to the experimental results of  $0.14\pi$  and  $0.19\pi$  obtained for  $\text{TbMnO}_3$  and  $\text{DyMnO}_3$ , respectively [20]. The pitch vector  $\mathbf{q}' = (0, k, 0)$  reported in the experiments translates to  $\mathbf{q} = (k/2, k/2, 0)$  on the Mn square lattice used here due to a  $45^\circ$  rotation between the two coordinate systems. The  $E$ -type AFM state has been observed in  $\text{HoMnO}_3$  [17,20].

For the larger Hund's rule coupling  $J_H$  the stability region of the spiral states shrinks considerably [see Fig. 3(b)]. Moreover, the spiral states are no longer sandwiched between the FM and the  $E$ -type phases. This implies that it is not possible in the commonly adopted double-exchange ( $J_H \rightarrow \infty$ ) limit to find transitions to spiral states as observed in  $RMnO_3$  upon varying the bandwidth, unless further interactions are added to the two-band model Hamiltonian.

The presence of a spiral structure in an insulator has been identified as one possible source for a spontaneous electric polarization  $\mathbf{P}$  by generating spin currents [11]. The direction of  $\mathbf{P}$  is perpendicular to both the direction of the spiral pitch vector  $\mathbf{q}$  and the cone axis of the spiral [12]. Our model of choice is isotropic in spin space and thus cannot determine the orientation of the cone axis relative to the crystallographic directions. Using the input from the experiments regarding the direction of the cone axis for the spiral state we indeed obtain the direction of  $\mathbf{P}$  consistent with the experiments [20,31]. Within the spin-current mechanism the magnitude of  $\mathbf{P}$  is controlled by the length of the pitch vector  $q$ , which we obtained in the experimentally relevant range.

Therefore our results verify that already the standard two-band model for manganites has all the necessary ingredients to sustain the magnetic spiral and the  $E$ -type phases as observed in the undoped perovskite manganites. A finite Hund's rule coupling of the order of the bandwidth

leads to a spiral pattern and a wavelength which both compare well with the observed magnetic structure in  $\text{TbMnO}_3$  and  $\text{DyMnO}_3$ . These results support the applicability of the spin-current mechanism as the source for ferroelectricity in  $RMnO_3$ . Lattice distortions of the  $\text{GdFeO}_3$  type are likely to give rise to additional longer-range couplings, which may further stabilize the spiral and the  $E$ -type states. The essential physics of these nontrivial spin states is already contained in the simpler short-range two-orbital model with finite  $J_H$ .

We thank E. Dagotto for useful comments. This work was supported by NanoNed, FOM, and by the Deutsche Forschungsgemeinschaft through SFB 484.

- 
- [1] For a review see D. Khomskii, *Physics* **2**, 20 (2009).
  - [2] R. Ramesh and N. Spaldin, *Nature Mater.* **6**, 21 (2007).
  - [3] C. Ahn, K. Rabe, and J.-M. Triscone, *Science* **303**, 488 (2004).
  - [4] N. Hill, *J. Phys. Chem. B* **104**, 6694 (2000).
  - [5] T. Kimura *et al.*, *Nature (London)* **426**, 55 (2003).
  - [6] N. Hur *et al.*, *Nature (London)* **429**, 392 (2004).
  - [7] G. Lawes *et al.*, *Phys. Rev. Lett.* **95**, 087205 (2005).
  - [8] T. Kimura, G. Lawes, and A. Ramirez, *Phys. Rev. Lett.* **94**, 137201 (2005).
  - [9] I. Sergienko, C. Sen, and E. Dagotto, *Phys. Rev. Lett.* **97**, 227204 (2006).
  - [10] S. Picozzi *et al.*, *Phys. Rev. Lett.* **99**, 227201 (2007).
  - [11] H. Katsura, N. Nagaosa, and A. Balatsky, *Phys. Rev. Lett.* **95**, 057205 (2005).
  - [12] M. Mostovoy, *Phys. Rev. Lett.* **96**, 067601 (2006).
  - [13] J. Betouras, G. Giovannetti, and J. van den Brink, *Phys. Rev. Lett.* **98**, 257602 (2007).
  - [14] D. Efremov *et al.*, *Nature Mater.* **3**, 853 (2004).
  - [15] J.-H. Kim *et al.*, *Phys. Rev. B* **78**, 245115 (2008).
  - [16] S. Seki *et al.*, *Phys. Rev. Lett.* **100**, 127201 (2008).
  - [17] T. Kimura *et al.*, *Phys. Rev. B* **68**, 060403(R) (2003).
  - [18] T. Goto *et al.*, *Phys. Rev. Lett.* **92**, 257201 (2004).
  - [19] E. Dagotto, *Nanoscale Phase Separation and Colossal Magnetoresistance* (Springer, Berlin, 2002).
  - [20] T. Kimura *et al.*, *Phys. Rev. B* **71**, 224425 (2005).
  - [21] S. Dong *et al.*, *Phys. Rev. B* **78**, 155121 (2008).
  - [22] T. Kaplan and S. Mahanti, arXiv:0904.1739.
  - [23] J. van den Brink and D. Khomskii, *Phys. Rev. Lett.* **82**, 1016 (1999).
  - [24] D.R. Neuber *et al.*, *Phys. Rev. B* **73**, 014401 (2006).
  - [25] M. Hamada and H. Shimahara, *Phys. Rev. B* **51**, 3027 (1995).
  - [26] D. Garcia *et al.*, *Phys. Rev. Lett.* **93**, 177204 (2004).
  - [27] D. Pekker *et al.*, *Phys. Rev. B* **72**, 075118 (2005).
  - [28] K. Pradhan and P. Majumdar, *Europhys. Lett.* **85**, 37 007 (2009).
  - [29] H. Aliaga *et al.*, *Phys. Rev. B* **64**, 024422 (2001).
  - [30] S. Kumar, A. P. Kampf, and P. Majumdar, *Phys. Rev. Lett.* **97**, 176403 (2006); *Phys. Rev. B* **75**, 014209 (2007).
  - [31] Y. Yamasaki *et al.*, *Phys. Rev. Lett.* **101**, 097204 (2008).